ANNALS OF GEOPHYSICS, 67, 2, VO217; 2024; Doi:10.4401/ag-9053
OPEN ACCESS

Investigating Mt. Etna lava fountains by seismic and infrasonic signals: 14-21 February 2021 case study

Javier Martínez Moreno[*,1], Andrea Cannata[2,3], Giuseppe Di Grazia[3], Mariangela Sciotto[3], Janire Prudencio Soñora[1]

(1) Department of Theoretical Physics and Cosmos, University of Granada, Avenida de la Fuente Nueva S/N, 18071, Granada, Spain
(2) Dipartimento di Scienze Biologiche, Geologiche e Ambientali, Università Degli Studi di Catania, Catania, Italia
(3) Istituto Nazionale di Geofisica e Vulcanologia, Osservatorio Etneo, Catania, Italia

Article history: Received November 29, 2023, Accepted June 15, 2024

Abstract

Infrasonic and seismic tremor are signals released by active volcanoes. These signals play a crucial role in monitoring volcanic activity and providing insights into volcanic dynamics and hazards. Between December 2020 and February 2022, Mount Etna was characterized by an intense eruptive period, during which monitoring efforts were employed to investigate the characteristics and source signals. Our work focuses on analyzing volcanic tremors in both seismic and infrasound signals to understand their behavior and relationship with the volcano's dynamics. In particular, the interval 14-21 February 2021, comprising 4 lava fountain episodes, was taken into account. Concerning the data analysis, amplitude, spectral content, seismic volcanic tremor and infrasonic explosion-quakes source locations have been computed. The results reveal that the seismic amplitude is closely related to emitted magma volume during the lava fountains. The study finds that most of the energy in volcanic tremors is concentrated below 5.0 Hz. During eruptive episodes, both seismic and infrasound signals exhibit lower frequencies, with variations between different stations due to propagation effects. Finally, two different source mechanisms of the seismic tremor were suggested: i) flow of gasses through a shallower permeable solid layer is likely to be responsible for the generation of volcanic tremor during non-eruptive periods; ii) magmatic flows along the shallow plumbing system and the consequent impact of particles on the walls of the conduit during eruptive periods.

Keywords: Mt. Etna; Volcanic tremor; Infrasonic tremor; Lava fountaining

1. Introduction

Active volcanoes are characterized by the generation of seismic and infrasonic signals throughout pre-eruptive, eruptive and post-eruptive periods. Analyzing these signals has become a vital tool for comprehending volcanic behavior, as they offer valuable insights into volcanic dynamics, fluid transport, local and regional stress conditions, and more [Ibañez and Carmona, 2000]. Furthermore, seismic signals have proven to be useful in forecasting potential future eruptions, as demonstrated in previous studies [Alparone et al., 2003; Konstantinou and Schlindwein, 2003].

On the other hand, infrasonic signals are particularly useful for investigating explosive processes and degassing [Sciotto et al., 2013].

The seismic signals emitted in volcanic environments can stem from shear failure processes, resulting in Volcano-Tectonic (VT) events, or they may be associated with processes that involve the internal fluids of the volcano, leading to long and very-long period events (LP and VLP, respectively) and tremor [Chouet, 1996; Cannata et al., 2013].

The importance of studying volcanic tremor lies in its close relationship with eruptive activity [e.g. Alparone et al., 2003; McNutt and Nishimura, 2008; Ichihara et al., 2016]. In basaltic volcanoes like Mount Etna, seismic tremor almost always accompanies eruptions [Battaglia et al., 2005; Konstantinou and Schlindwein, 2003; Cannata et al., 2013]. Seismic tremor can last from several minutes to hours, or even months [Steinberg and Steinberg, 1975; Chouet, 1996; Chouet and Matoza, 2013; Sciotto et al., 2022a]. Normally, the origin of seismic tremor has been associated with several source mechanisms such as fluid-elastic resonance and frictional processes [see Girona et al., 2019 and references therein]. The dominant frequency recorded in seismic tremor waves falls within

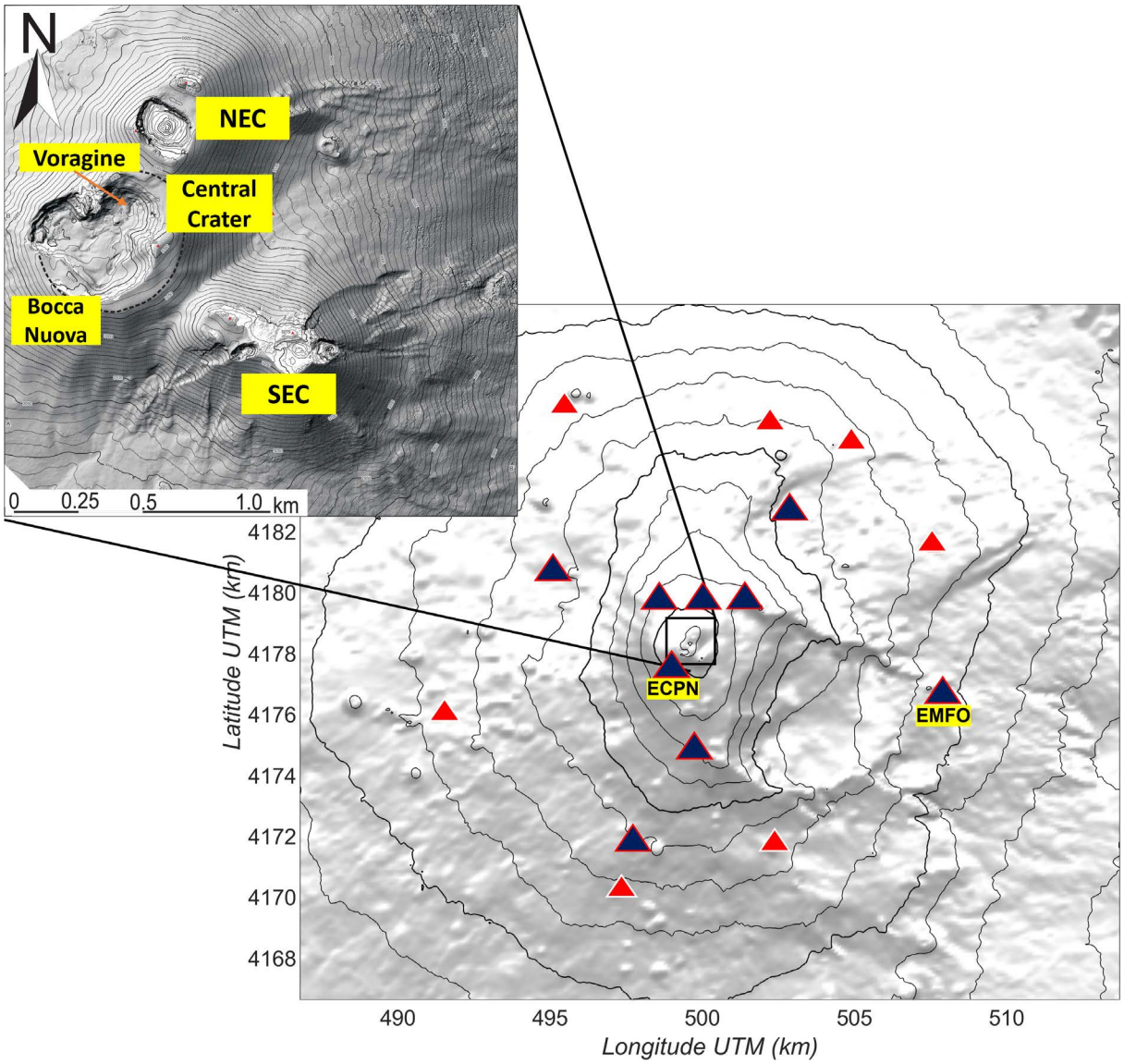

Figure 1. Mount Etna map view. The main image shows a complete view of Etna volcano, with 9 blue triangles which represent stations with co-located infrasound and seismic sensors and 7 red triangles which represent seismic stations. The image in the upper left corner displays the volcano summit area where the main craters are present [from Neri et al., 2017]. Most of the analyses shown in the paper were performed on the signals recorded by stations ECPN and EMFO.

the range of 0.1 to 15 Hz [Alparone et al., 2007; Cannata et al., 2008; Girona et al., 2019]. Almendros et al. [1997] assume that these low-frequency peaks are due to effects of the tremor's source, while other studies [e.g., Gordeev, 1993; Benoit and McNutt, 1997; Mora et al., 2001] consider the possibility that path effects are responsible for this behavior in the spectrum of volcanic tremor.

Active volcanoes frequently produce infrasonic signals, which are sound waves with frequency below 20 Hz [Matoza et al., 2009; Fee et al., 2010; Fee and Matoza 2013; Matoza and Roman, 2022]. These signals originate from subsurface and subaerial zones and are associated with processes such as explosive activity, degassing, pyroclastic flows, and rock avalanches [Matoza and Roman, 2022; Sciotto et al., 2013]. Infrasonic signals play a crucial role in volcano monitoring as they contribute to the understanding of volcanic processes, investigation of eruption dynamics, assessment and mitigation of volcanic hazards, comprehension of eruptive column physics [Johnson et al., 2004; Johnson and Ripepe, 2011; Fee and Matoza, 2013], and reconstruction of magma conduit geometry through resonance [Fee et al., 2010; Sciotto et al., 2022b], among other applications. Among these infrasonic signals, infrasonic tremors can persist for minutes to days and are primarily generated by degassing and explosive activities [Cannata et al., 2013].

This article aims to analyze seismic and infrasound tremor generated at Mount Etna during the week of February 14th to 22nd, 2021. This week is part of an eruptive period that extended from December 13th, 2020, to February 21st, 2022, during which a total of 66 lava fountain episodes were recorded [Calvari and Nunari, 2022]. Within the week of activity examined in this study, four eruptive episodes occurred on February 16th, 17th-18th, 19th, and 20th-21st at the Southeast Crater (located at an altitude of 3.340 meters above sea level and referred to as SEC henceforth; Fig. 1). As already evidenced by Andronico et al. [2021], the time-interval between consecutive lava fountain episodes gradually increased. This behavior was previously observed at Mt. Etna, such as in 2000 [Alparone et al., 2003] and in the first half of 2013 [Spampinato et al., 2015]. All eruptions during this period were characterized by an initial increase in Strombolian activity, followed by the formation of powerful lava fountains that gradually waned until the conclusion of each event [Andronico et al., 2021]. In this article, the primary focus will be on the analysis of volcanic tremor in both infrasonic and seismic signals. Additionally, explosion-quakes with both seismic and infrasonic components will be investigated. The objective of this study is to establish connections between the behavior and variations of seismic and infrasound signals and the dynamics of the volcano.

2. Material and methods

2.1 Data

The data used in this document have been collected by the permanent network of seismic and infrasound stations run by the INGV-OE (Istituto Nazionale di Geofisica e Vulcanologia – Osservatorio Etneo). The part of the network used to analyze seismo-volcanic and infrasonic signals generated by Mt. Etna consists of sixteen stations, of which seven collect only seismic signals, and the remaining nine record both seismic and infrasound signals [Sciotto et al., 2022a]. All these stations were used for source location of both volcanic tremor and explosion-quakes, while only two seismo-acoustic stations, ECPN (2.996 meters above sea level) and EMFO (1.163 meters above sea level), located southwest and east of the main craters respectively, were used for amplitude and spectral analyses (Fig. 1). These two stations have been chosen for two main reasons: the geographical position and the good quality, in terms of signal to noise ratio, of the collected signals.

The selected seismic stations are equipped with Nanometrics Trillium (40 s cut-off period) three-component broadband seismometer with a sampling frequency of 100 Hz, while, concerning the infrasonic stations, GRASS 40AN microphones with a flat response and a sensitivity of 50 mV/Pa in the frequency range of 0.3-20,000 Hz are installed [Calvari et al., 2022; Andronico et al., 2021; Sciotto et al., 2022b; Patanè et al., 2013; Cannata et al., 2013].

2.2 Methods

To study the signals gathered by EMFO and ECPN stations, four different processing techniques have been carried out: i) seismic and infrasound amplitude calculation using the Root-Mean-Square (RMS) amplitude; ii) spectral analysis using Fast Fourier Transform to explore frequency variation by using spectrograms, frequency peak and

mean frequency; iii) explosion-quakes location (only for the infrasonic components); iv) volcanic tremor source localization.

The amplitude plays a fundamental role in the analysis of seismic and infrasonic signals from volcanoes and in understanding their temporal evolution. By using amplitude measures [RSAM or RMS; e.g., Endo and Murray, 1991; Battaglia and Aki, 2003], significant patterns and trends in the seismic signals can be detected, which provide valuable information about the inner activity of the volcano [e.g., McNutt and Nishimura, 2008; Ichihara et al., 2016; Andronico et al., 2021]. To calculate the RMS amplitude, data from both seismic and infrasound signals collected by EMFO and ECPN stations have been used. The computation has been performed on 10.24-second-long non-overlapping windows of signal, filtered in the frequency band 0.5-5.5 Hz. This band was chosen on the basis of the most common frequency content of volcanic tremor at Mt. Etna [Cannata et al., 2010].

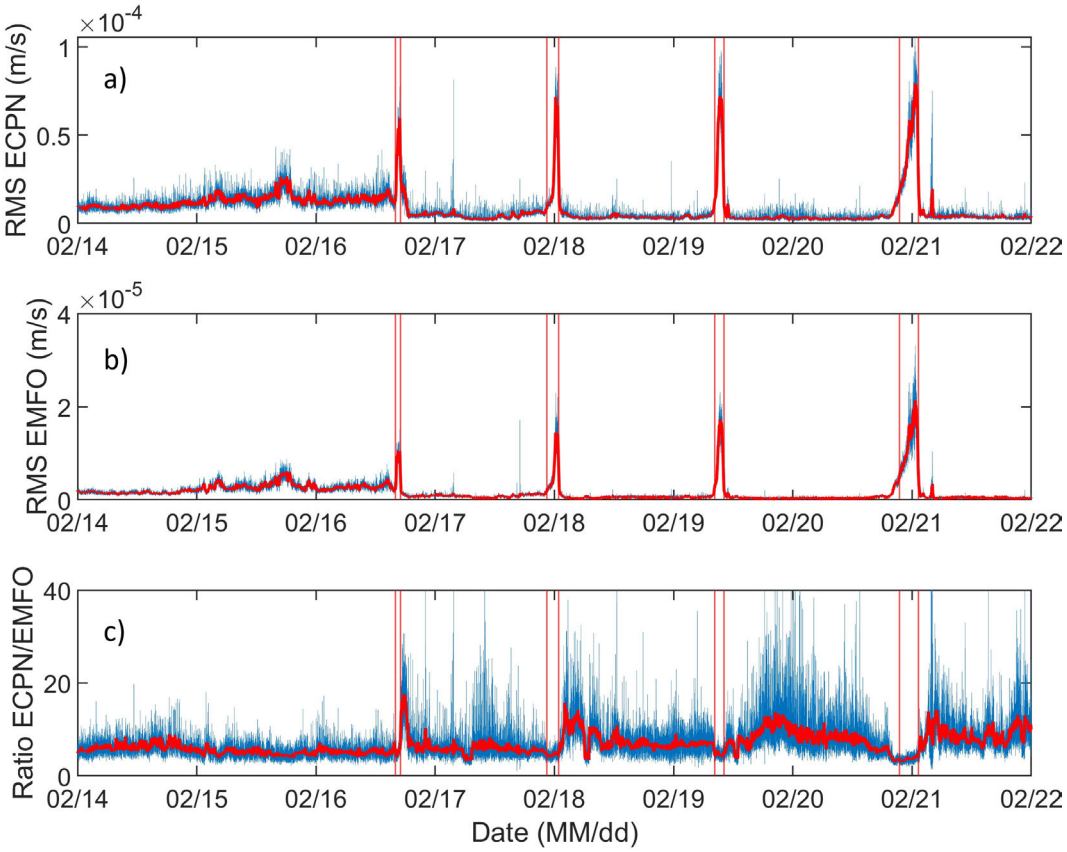

Figure 2. Time variation of the RMS amplitude computed on the vertical component of the seismic signals acquired by ECPN (a) and EMFO (b) stations, and ratio between these (c). The times of occurrence of the lava fountain episodes are marked by red vertical lines. In each plot, the thick red line represents the 40-min-long moving average.

Also for the spectral analysis we focused on ECPN and EMFO stations as they provide "examples" of Etna volcanic tremor as recorded by stations located closer to and more distant from the summit craters. The spectral analysis of the seismic signals has been performed using Fast Fourier Transform (FFT) in time windows of 40.96 seconds. First of all, spectrograms and normalized spectrograms were calculated for the vertical component of the seismic signals recorded by ECPN and EMFO stations. In addition, with the aim of observing changes in the predominant frequencies of the seismic signals, per each spectrum both peak frequency and mean frequency have been calculated [e.g., Carniel et al., 2005; Sciotto et al., 2022a]. The computing of the frequency peaks involves identifying and extracting the frequency values with the highest spectral amplitudes. As for the mean frequency, it is obtained by calculating the weighted mean of the overall frequency distribution [e.g., Carniel et al., 2005]. This average value provides information about the central or typical frequency in the amplitude spectrum.

On February 21st, the seismic-infrasound station network recorded a series of explosion-quakes. The location of these events was estimated by using a two-dimensional grid-search approach (with a grid of 6x6 km and a grid step of 0.05 km) based on the brightness function [Kao and Shan, 2004; Cannata et al., 2013]. Infrasound transients are band-pass filtered in the range 0.5-5 Hz, and the method consist in finding a set of arrival times yielding the maximum value of the brightness function, which is obtained when the largest amplitudes at the stations have been aligned.

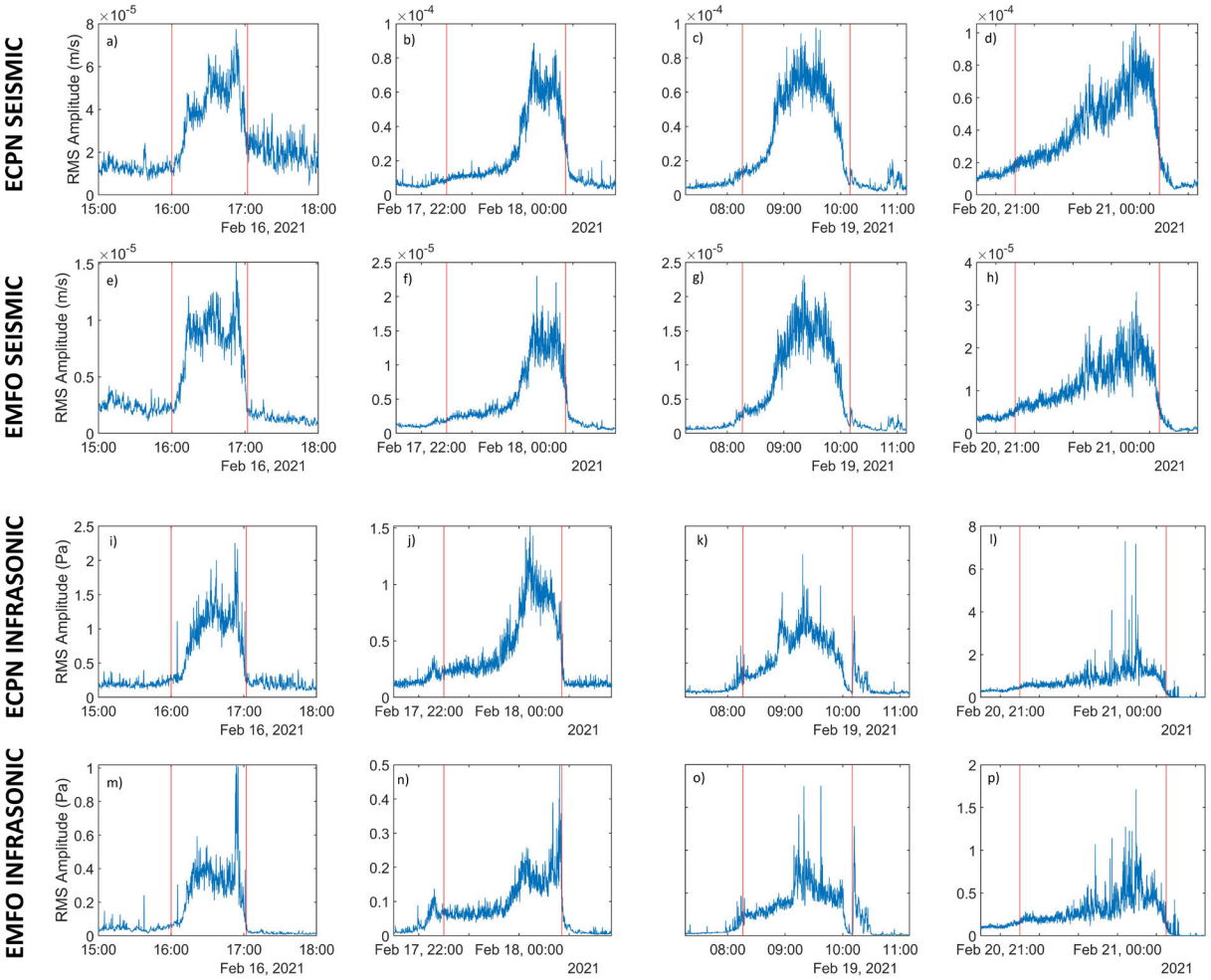

Figure 3. Time variation of RMS amplitude for each eruptive episode calculated at the vertical component of the seismic signal acquired by ECPN (a-d) and EMFO (e-h) stations and RMS amplitude for each eruptive episode calculated on the infrasound signals acquired by ECPN (i-l) and EMFO (m-p) stations. The times of occurrence of the lava fountain episodes are marked by red vertical lines.

To compute the locations of volcanic tremor sources, a three-dimensional grid-search approach method has been employed with a grid size of 6x6x6 km and a grid step of 0.25 km. This method relies on the decay of seismic amplitude with distance and assumes the propagation of seismic waves in a homogeneous medium [for more details, refer to Di Grazia et al., 2006; Cannata et al., 2013]. Tremor source locations were estimated using 10-minute non-overlapping windows filtered in the 0.5-2.5 Hz frequency band. This is the band routinely used to perform volcanic tremor source location at Mt. Etna [Cannata et al., 2013]. Volcanic tremor source locations are retrieved by using all the 16 seismic stations shown in Figure 1, as in this method the location accuracy improves with an increasing number of stations, resulting in reduced errors in tremor source localization. Once the volcanic tremor locations were constrained, we also computed the seismic reduced amplitude, that is the seismic amplitude reduced at 1 km from the tremor source.

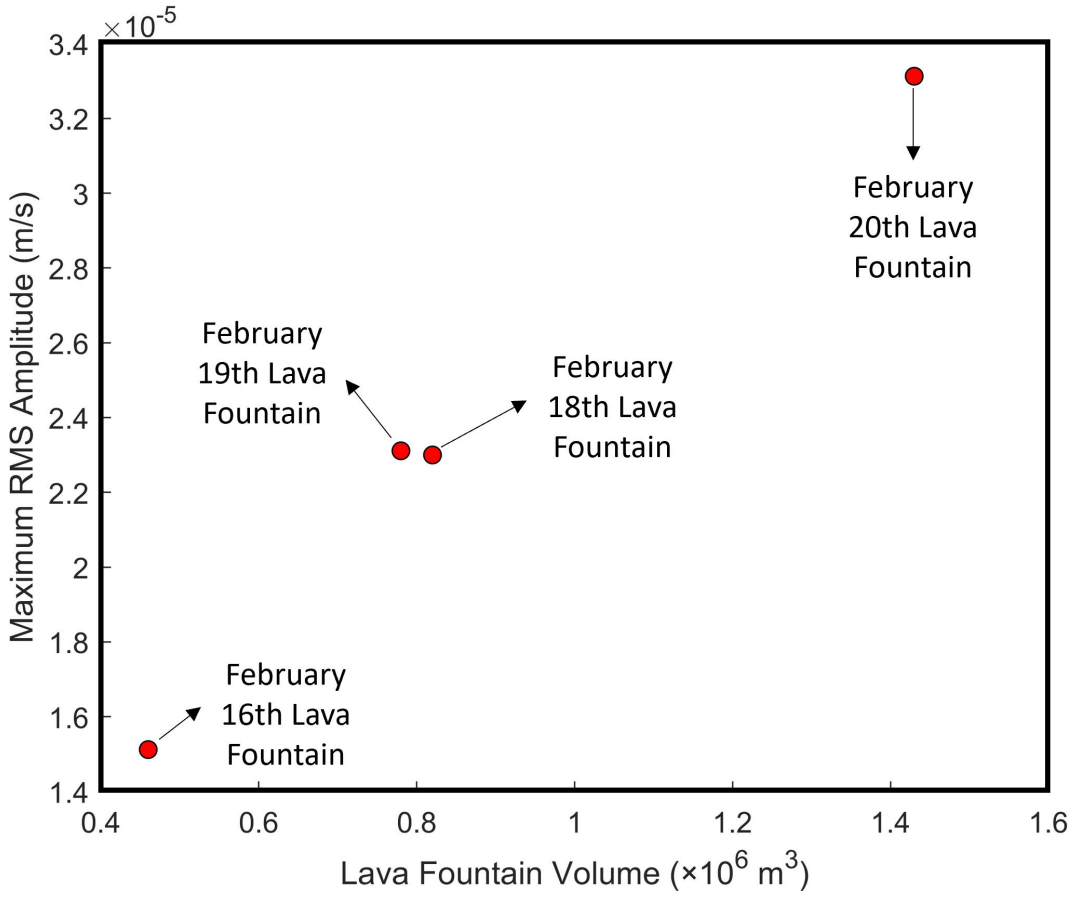

Figure 4. Maximum RMS amplitude, calculated on the vertical component of the seismic signal recorded by EMFO station during the 4 lava fountain episodes, versus the volume of magma provided by Calvari and Nunnari [2022].

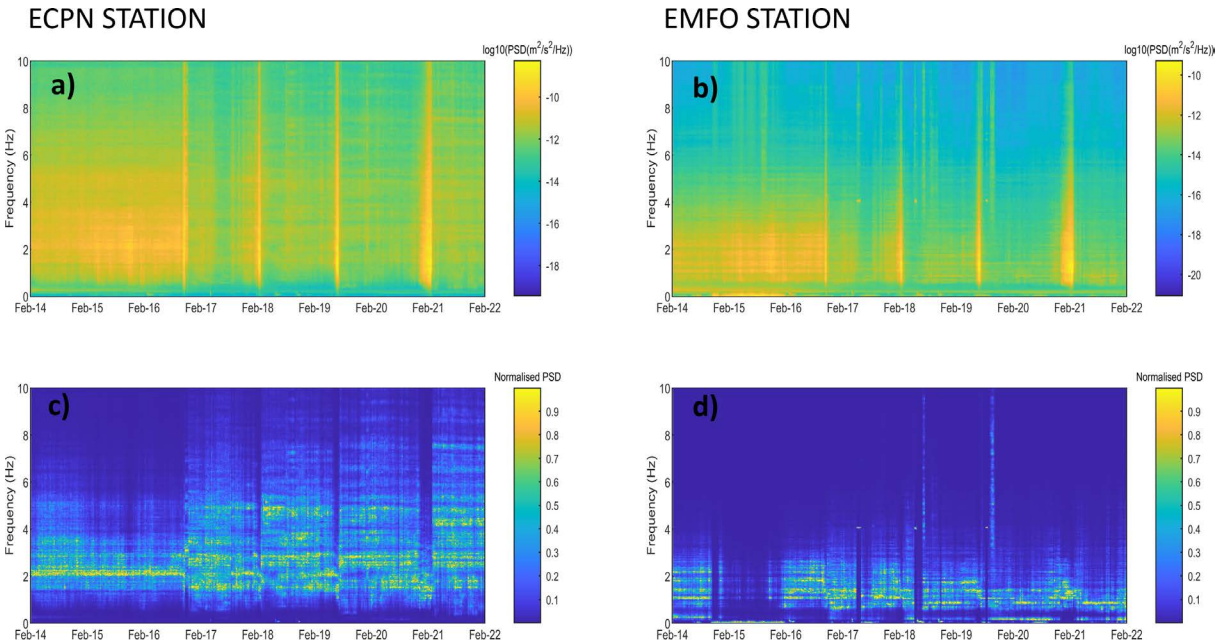

Figure 5. Spectrograms and normalised spectrograms of the vertical component of the seismic signals recorded by ECPN (a,c) and EMFO (b,d) from 14 to 21 February 2024 calculated by using a non-overlapping 40.96-sec-long window.

3. Results and discussion

3.1 Seismic signals

The first notable aspect of Figures 2a,b and 3a-h is the very high level of volcanic tremor amplitude during the initial period, before the sequence of lava fountains (February 14th to 16th), which is uncommon in Mount Etna. In addition, a sharp increase in tremor amplitude is observed during each paroxysmal event, which can be attributed to the increasing release of energy during periods of explosive activity. The movement of large magma volumes within the volcano is a clear causal factor in the generation of significant seismic amplitudes during lava fountains. Indeed, following the model proposed by Gestrich et al. [2020], the impact of particles on the walls of volcanic conduits can be identified as one of the source mechanisms of the volcanic tremor during explosive periods. On the basis of this model, the seismic efficiency of this process strictly depends on grain size and/or wall roughness. Another interesting point illustrated by the graph is how the maximum amplitude of each paroxysmal episode is lower than that of the subsequent episode (with the exception of the second and third, 18th and 19th February, respectively, when the amplitudes are very similar). A gradual increase of RMS amplitude for each lava fountain over time was also observed in other eruptive periods on Mount Etna, such as the 2013 episodes documented by Spampinato et al. [2015]. This pattern could be due to the increase in the volume of magma emitted during the episodes as suggested by Calvari & Nunnari [2022] (Fig. 4). It is worth noting how this increasing trend observed in the seismic amplitude for the lava fountains from 16 to 21 February has not been observed in other data available in literature such as the lava fountain height and the time averaged discharge rate [provided by Calvari and Nunnari, 2022] and the measurements collected from the Spinning Enhanced Visible and InfraRed Imager

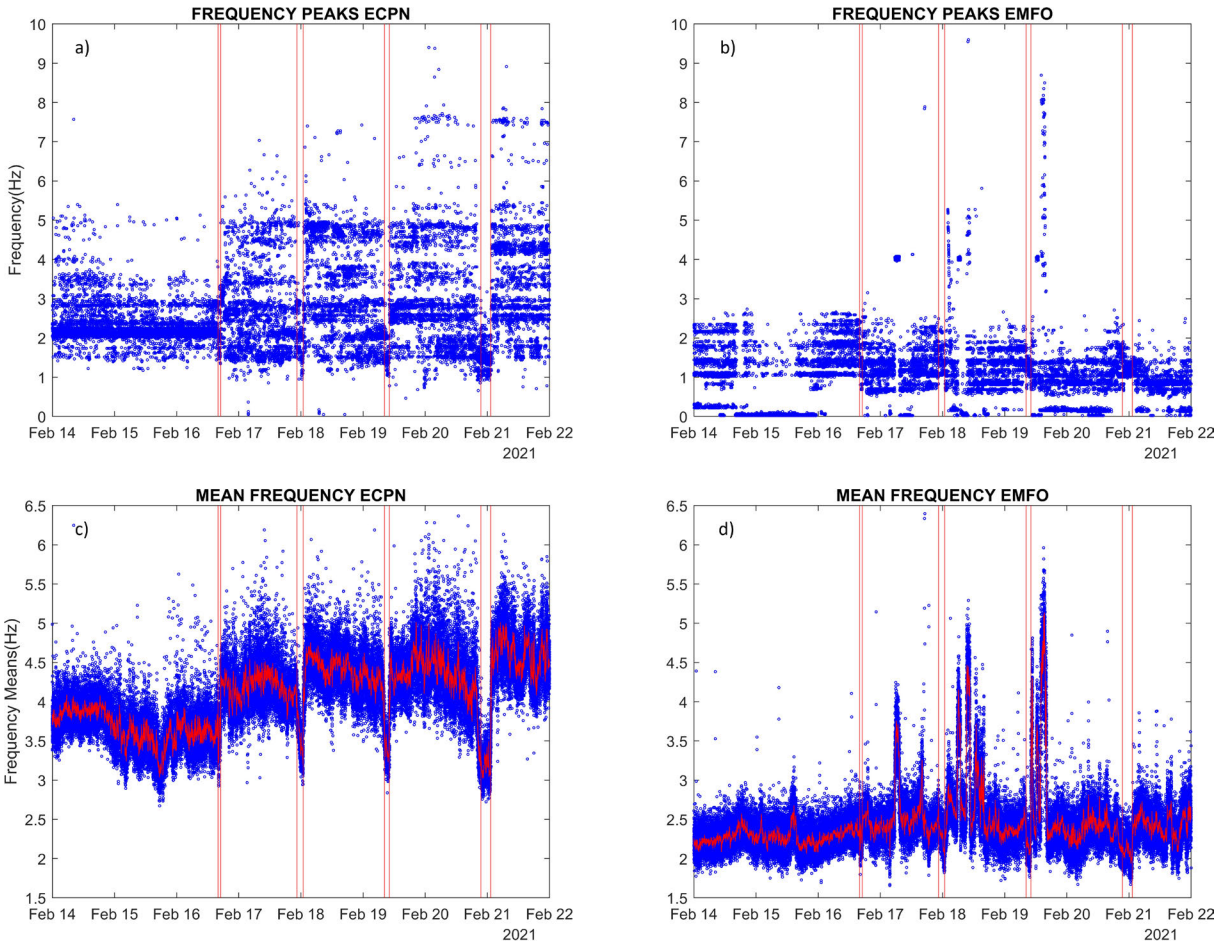

Figure 6. Frequency peaks and mean frequency variations in time computed on the seismic signals acquired by ECPN (a,c) and EMFO (b,d). The times of occurrence of the lava fountain episodes are marked by red vertical lines. The thick red lines in (c,d) represent the 40-min-long moving average.

(SEVIRI) instrument [volcanic cloud top height and ash/ice/SO_2 masses in Guerrieri et al., 2023; radiative energy in Marchese et al., 2021]. In addition, it can also reasonably be assumed that during so close in time explosive episodes an enlargement of the shallowest portion of the conduit/vent takes place. This hypothesis has been also invoked to interpret the low energy of the first eruptive episode of the 2011 SEC lava fountains [Sciotto et al., 2019]. As shown by McNutt and Nishimura [2008], the amplitude of volcanic tremor linearly increases with crater radius.

With the aim of analyzing possible relative shifts of the volcanic tremor source, the ratio between the seismic amplitudes at ECPN and EMFO stations has been computed. In Figure 2c, the RMS ratio ECPN/EMFO can be visualized. It can be observed that this ratio remains stable at low values from the beginning of the analyzed period until the end of the first lava fountain. However, after this first episode, the ratio experiences a drastic increase. Following this initial lava fountain, all subsequent fountains exhibit similar patterns in the seismic ratio: a clear decrease at the beginning of each explosive episode, and a sharp increase at the end of each episode. The seismic ratio behavior can be explained by taking into account the position of both stations with respect to the location of volcanic tremor sources. ECPN station is located near the summit of Mt. Etna, southwest of the craters, while EMFO station is situated on the flank of the mountain, southeast of the summit. The proximity of ECPN station to the summit area of the volcano allows it to record volcanic tremor signals with much higher amplitude than those gathered by EMFO station. During the period prior to the first eruption and during it, the low RMS ratio suggests that the volcanic tremors are localized in the SEC area, closer to the EMFO station than during the time intervals between lava fountains. In particular, during these intervals between lava fountains the tremor sources migrate northwestward towards the center of the summit area and, then, an increase in the ECPN/EMFO RMS ratio is observed. During the paroxysmal events following the first lava fountain, the ratio undergoes a considerable decrease, suggesting (as will be discussed in the tremor source location section) that the sources of the volcanic tremor during eruptive phases shift back southeastward towards the SEC, leading to a decrease in the ratio between ECPN/EMFO.

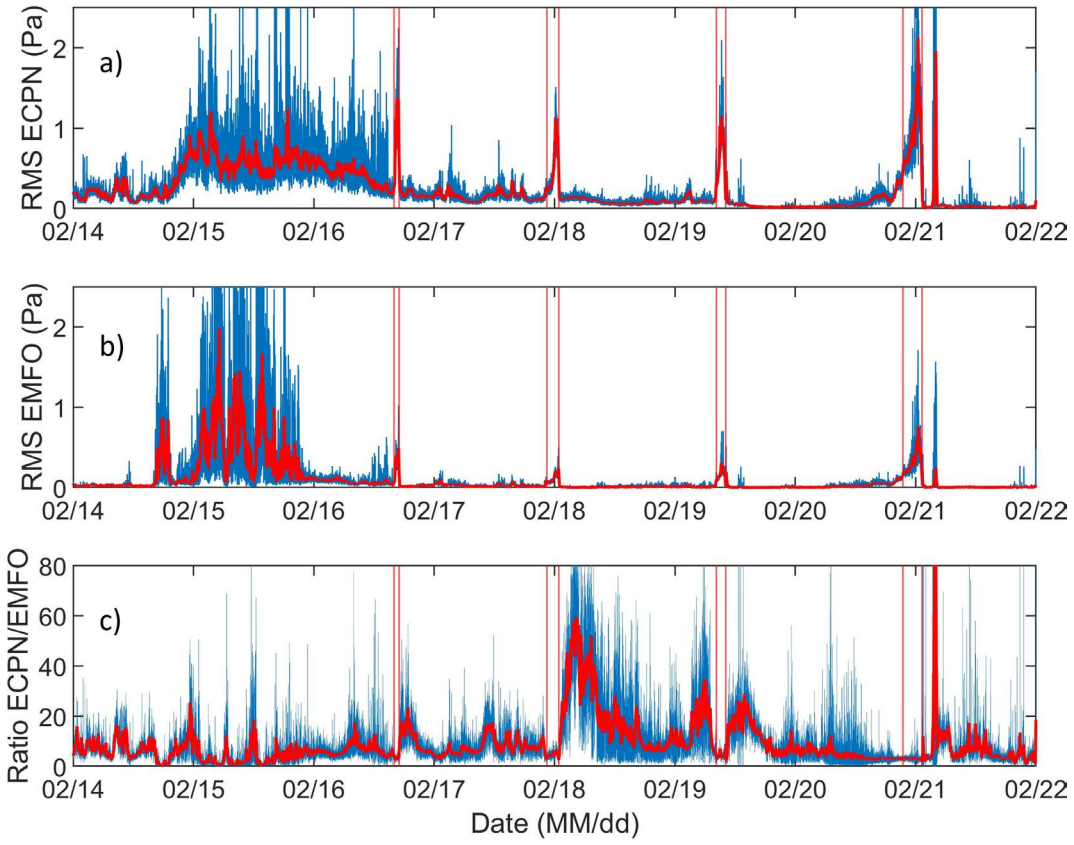

Figure 7. Time variation of the RMS amplitude computed on the infrasound signals acquired by ECPN (a) and EMFO (b) stations, and ratio between these (c).The times of occurrence of the lava fountain episodes are marked by red vertical lines. In each plot, the thick red line represents the 40-min-long moving average.

In Figure 3 it is possible to appreciate in a more precise way the RMS amplitude calculated for each station in the 4 windows of the eruptive events. The start and end of each episode are marked with red vertical lines. The start and end times of each lava fountain were obtained from Calvari and Nunnari [2022] and from the bulletins published by INGV (https://www.ct.ingv.it/index.php/monitoraggio-e-sorveglianza/prodotti-del-monitoraggio/bollettini-settimanali-multidisciplinari). Given that the pattern of the RMS amplitude time series in each lava fountain is almost identical in both stations (with only the amplitude level varying), when referring to the "shape" of the seismic signal, we will refer to the episodes of February 16th, 17th-18th, 19th, and 20th-21st, respectively labeled 1st, 2nd, 3rd, and 4th, without mentioning the station. A common trend in the four studied episodes is the increase in volcanic tremor amplitude at the beginning of the eruptive activity. In the first episode (Fig. 3a,e), the increase in amplitude is sudden while in the 2nd and 3rd episodes (Fig. 3,b,f,c,g), the amplitude increase occurs in two distinct phases: the first phase is characterized by a gradual increase, and the second phase exhibits an abrupt increase. The absence of a gradual increase in the RMS amplitude in the initial lava fountain can be attributed to the high levels of the background volcanic tremor amplitude and the ongoing strombolian activity. Finally, during almost the entire duration of the 4th lava fountain episode (Fig. 3d,h), there is a gradual increase in seismic amplitude which lasts from the onset to the climax of the lava fountain, from 21:30 to 00:58, after which there is a sharp decrease of the seismic signal amplitude up to the end of the event at 01:15. The 4th event is the most characteristic, both for its morphology and for being the event with the highest amplitude and longest duration. Regarding the cessation of paroxysmal activity (second vertical line of each window), a common behavior is observed in the four events: the end of the lava fountains coincides with a sudden decrease in amplitude to values similar to those before the start of the activity.

Although the boundaries between Strombolian and paroxysmal phases are not well defined, it is possible to approximate, in a general way and following the morphology of the RMS amplitude time series, the beginning and end of each phase of the eruptive phenomena. Following the comparison between the temporal variation of the volcanic tremor amplitude and the time evolution of the volcanic phenomena performed by Alparone et al. [2003], it is observed that the RMS amplitude of the seismic signals starts to increase at the onset of the Strombolian activity. It reaches its maximum value during the development of the lava fountain and the paroxysmal phase. Subsequently, the amplitude of the seismic signals begins to decrease, and it returns to a "normal" level at the end of the explosive activity. Hence, as highlighted by previous works [Andronico et al., 2021 and references therein], the amplitude of the seismic signal, dominated by the volcanic tremor at Mt. Etna, can be considered a proxy of the explosive activity, and for this reason is used as one of the most important parameters in the Etna lava fountain early warning systems [D'Agostino et al., 2013; Cassisi et al., 2016; Cannavò et al., 2017; Langer et al., 2022]. For the same reason, at Mt. Etna as well as in other volcanoes, seismic signal amplitude has also been used to try to constrain eruption source parameters such as plume height [Fee et al., 2017], lava fountain height [Sciotto et al., 2019], magma discharge rate [Ichihara et al., 2016] and eruptive "magnitude" [i.e., erupted volume; Calvari et al., 2022].

To study the spectral content of the volcanic tremor, spectrograms, peak frequencies and mean frequencies of the seismic signals were computed. The Figures 5 and 6 show that most of the energy of the volcanic tremor is confined below 5 Hz, in agreement with what reported in literature [e.g. Lombardo et al., 1996; Falsaperla et al., 2005; Cannata et al., 2010]. The usual pattern during the lava fountain episodes follows a trend towards lower frequencies during the paroxysmal phases, in the frequency bands 1.0-3.0 Hz and 1.0-2.5 Hz, in the case of the ECPN and EMFO stations, respectively. The frequency peak data, obtained from the information collected by the ECPN station during the period prior to the eruption on February 16th, exhibit a predominance of frequencies in the 2 Hz range. These frequencies remain stable within that range until the onset of the first lava fountain. However, the tremor depicts a more broadband nature after the first event, during the periods between paroxysmal episodes, when the frequency peak values turned out to be more spread over the band 1.5-6.0 Hz (Fig. 6a). The mean frequency (Fig. 6c,d) more clearly shows the decrease in the tremor dominant frequency during the paroxysmal events. Indeed, for both stations, during eruptive periods, mean frequency values tend to decrease, with a range of 2.8-4.0 Hz for ECPN and 1.7-2.7 Hz for EMFO.

It is also worth noting that both peak frequencies and mean frequencies during eruptive episodes are significantly lower at the EMFO station compared to the ECPN station. This can be explained through anelastic attenuation, which depends, among other factors, on the wave frequency [Pulli, 1984]. In particular, the higher the frequency, the stronger the attenuation. Since EMFO station is located further away from the source of volcanic tremors compared to the ECPN station, it is expected that high-frequency waves have experienced greater anelastic attenuation, resulting in a lower frequency content.

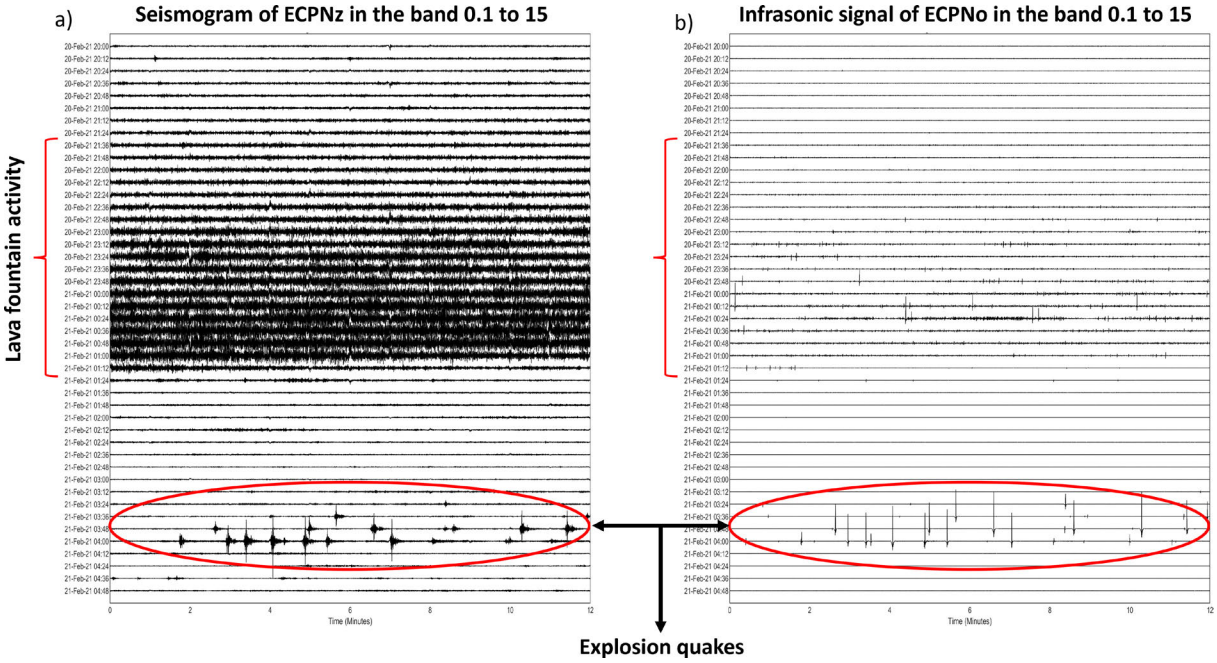

Figure 8. Seismogram (a) and infrasonic (b) signals from ECPN station for February 20th-21st, spanning from 20:00 to 05:00, are shown in this image. It includes seismic vertical (a) and infrasound (b) recordings. Two red brackets highlight the lava fountain period and two red ellipses indicate the explosion-quakes that occurred after the end of the lava fountain.

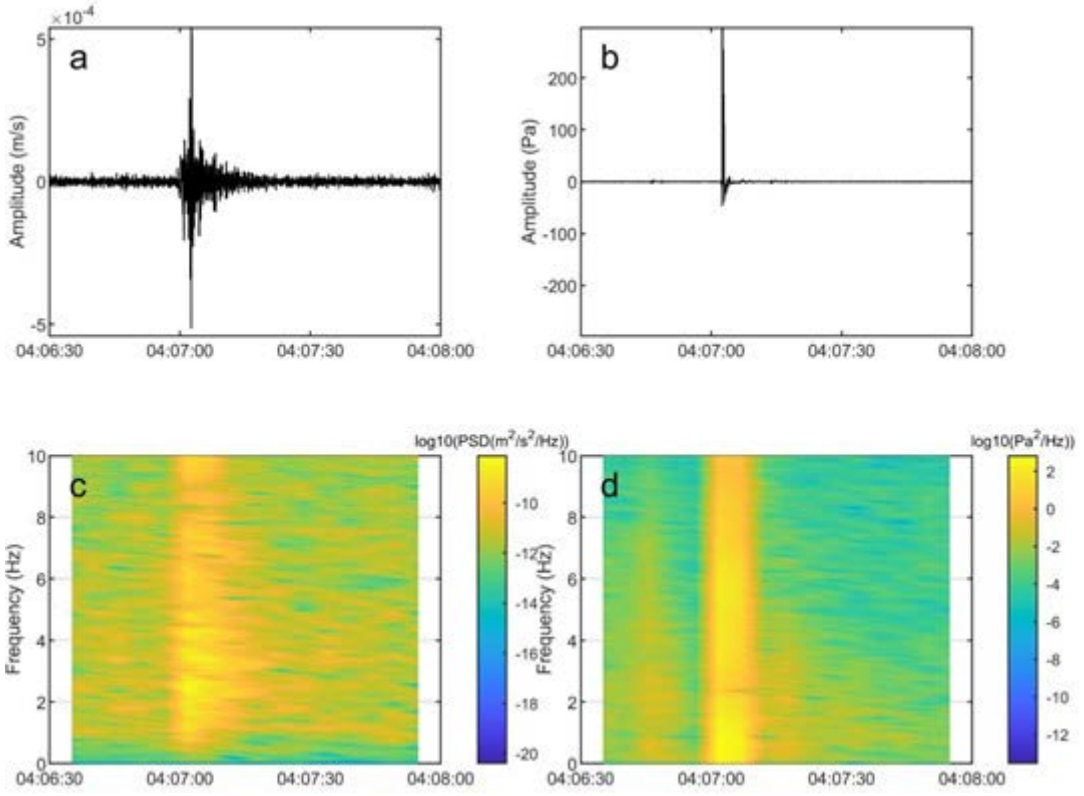

Figure 9. Seismic and infrasonic waveforms (a,b respectively) of an explosion-quake, that occurred on 21 February 2021 after the end of the 4th lava fountain, recorded by ECPN station and corresponding spectrograms (c,d), obtained by using 10.24-s-long windows with an overlap of 5.12 s.

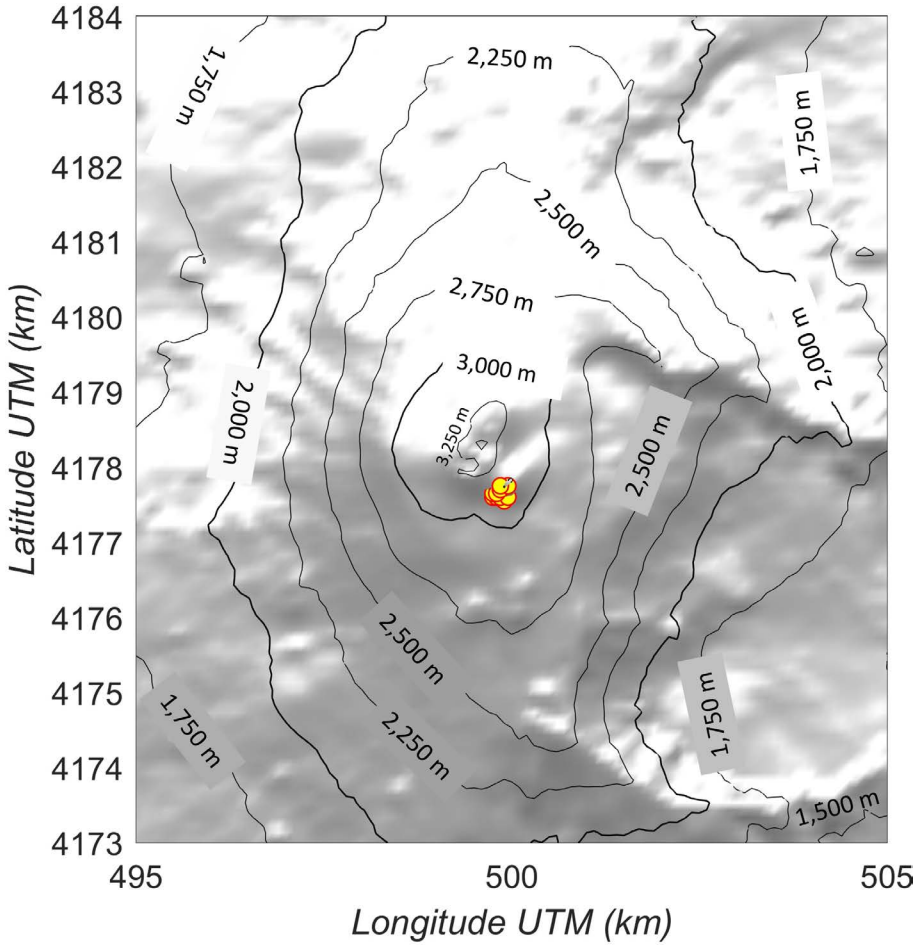

Figure 10. Digital elevation model of Etna, with the locations of the infrasonic component of the explosion-quakes that occurred on February 21st from 03:30 to 04:15 (yellow and red circles; see Fig. 8).

In a discontinuous but consistently present manner throughout all the recorded data, very low values (<0.5 Hz) are observed in the peak frequency recorded by EMFO station (Fig. 6b). The continuous presence of phreatic layers in the subsurface of Mount Etna [D'Alessandro and Vita, 2003] and the consequent movement and oscillation of water masses near that station may be a direct cause of these abnormally low frequencies, aligning with the relationship

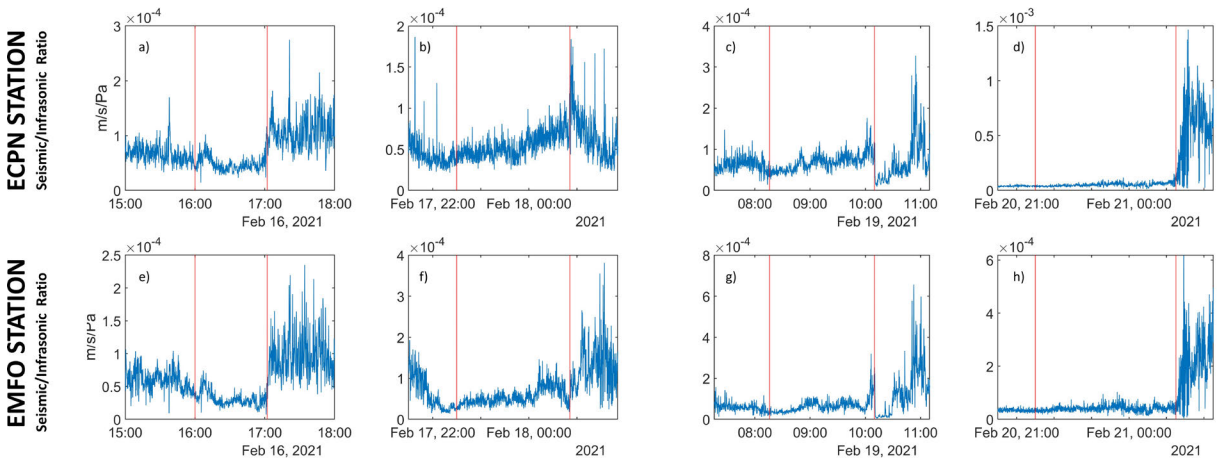

Figure 11. Time variation of seismic/infrasonic RMS amplitude ratio for each eruptive episode acquired by ECPN (a-d) and EMFO (e-h) stations. The times of occurrence of the lava fountain episodes are marked by red vertical lines.

between low frequencies of seismic signals and aquifers as also suggested by other authors [e.g., Buzzard et al., 2023; Tribaldos and Ajo-Franklin, 2021]. Another possible explanation of these local very low frequency noise at EMFO station could be seismic site effects due to the local shallow loose volcanic material.

Furthermore, it can be noted in both peak and mean frequency time series from EMFO that sudden increases in frequency took place on February 17, 18, and 19 (Fig. 6b,d). In order to understand the meaning of these frequency increases, seismograms obtained from data collected by each station were visually inspected to identify possible anomalies. High-frequency transient signals were found during those time periods, and there was no evidence of volcanic-seismic activity, hence those signals were associated with anthropogenic seismic noise unrelated to volcanic activity.

3.2 Infrasonic signals

Similarly to the time series of the seismic RMS amplitude, a significant amplitude is observed in the infrasound signals at the beginning of the data series, during the first pre-eruptive period (Fig. 7a,b). Hence, such high seismo-acoustic energy, suggesting sources coupled with both rocks and atmosphere, could be related to intense degassing processes/mild explosive activity. Also, the trend followed by the infrasound amplitude since the first eruptive episode is similar to that followed by the seismic amplitude: a drastic increase in amplitude at the beginning of each eruptive period due to explosions, followed by a decrease in the periods between eruptions, when the acoustic pressure produced by volcanic phenomena decreases to values very close to zero. However, the maximum amplitude of the acoustic pressure does not increase chronologically during all the four lava fountain episodes, as observed in the seismic amplitude, but only in the last three episodes. It has to be noted that infrasonic amplitude is strongly affected by factors such as topography and atmospheric parameters [especially wind; e.g. Iozzia et al., 2023], that have a much lower influence on the seismic amplitude.

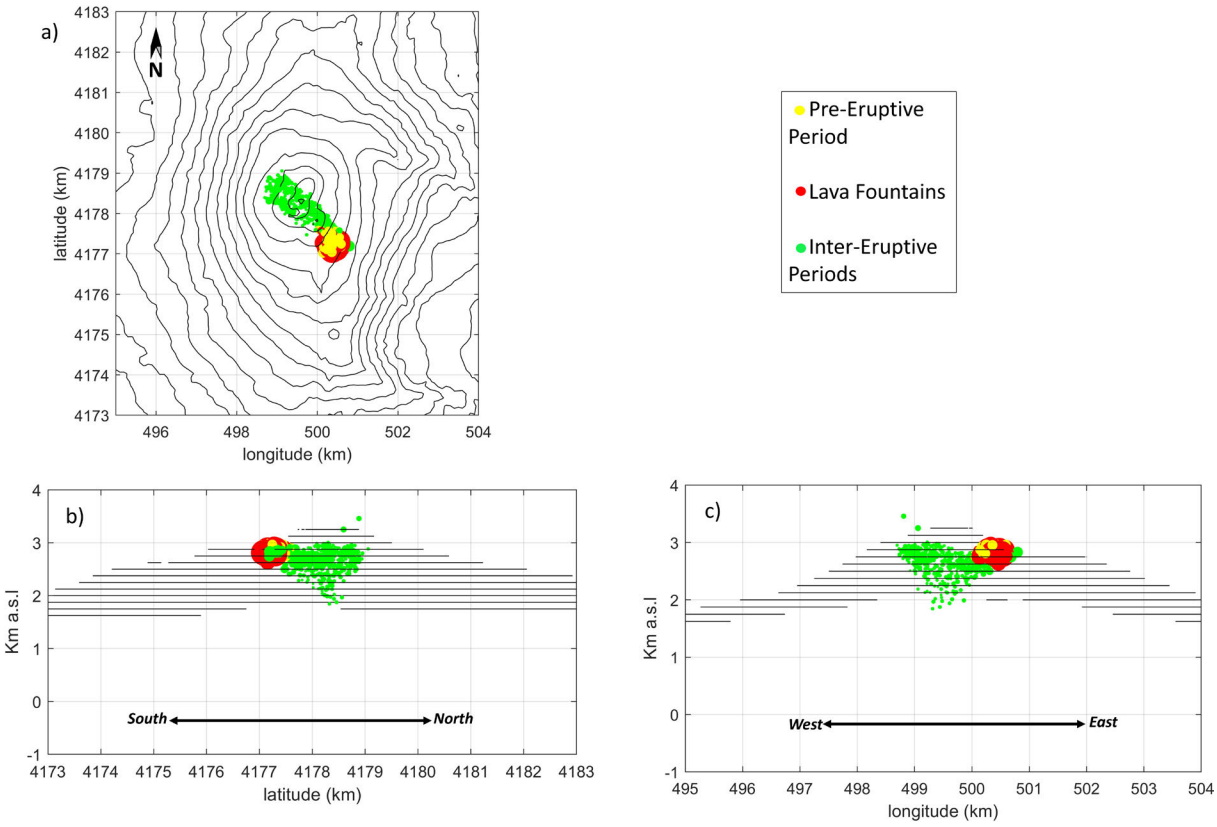

Figure 12. Seismic tremor source locations shown in map (a) and sections (b,c) of Mount Etna. The locations of the tremor sources are represented by dots of varying sizes (depending on the seismic reduced amplitude) and colors (depending on time, see the legend in the upper right corner). Due to technical issues in some stations, tremor source locations on February 14th have not been computed.

The ratio between the infrasound signal amplitude at ECPN and EMFO (Fig. 7c) exhibits an entropic behavior with few stable values. The clearest trend followed by the ratio is observed during paroxysmal events, when it remains at very low values steadily until the end of each lava fountain, when the ratio dramatically increases. The unclear patterns observed in the ratio during the non-eruptive periods can be due to the fact that, unlike the seismic signals, the infrasonic signals are dominated by local noise sources (such as wind, especially for high altitude stations) when the volcano does not show explosive activity.

When focusing on the trend of RMS amplitude of the infrasonic signals for each paroxysmal episode (Fig. 3i-p), a notable similarity is observed in relation to the pattern exhibited by the seismic amplitude across all lava fountains in terms of shape of the RMS amplitude time series. On the other hand, during each paroxysmal episode, spikes in the infrasonic RMS amplitude have been recorded that have not been so clearly observed in the seismic RMS amplitude time series. The most evident examples of these "anomalies" in the infrasonic signal have been recorded towards the end of the lava fountain on February 19th (Fig. 3k,o), but, notably, these high-amplitude peaks are present throughout almost the entire eruptive period during the night of February 20th and 21st (Fig. 3l,p). These could be attributable to an intense explosive source located in an open conduit, in correspondence with the fragmentation level (Fig. 8).

After the last paroxysmal episode, a significant increase in amplitude was observed during a short period of time in both seismic and infrasound signals of both stations (Figs. 2 and 7). The seismic and infrasonic recordings show the presence of amplitude transients between 03:30 and 04:15 on February 21st (Fig. 8), that are explosion-quakes associated with post-lava fountain Strombolian activity (an example is shown in Fig. 9). The infrasonic components of these events have been located within the SEC (Fig. 10). The magma is directly involved in this type of shallow processes [Patanè et al., 2004], and the explosions may be related to the ascent of rapidly expanding gas bubbles that fragment the surrounding medium [Pioli et al., 2022]. The occurrence of Strombolian activity subsequent to the cessation of eruptive activity is not an uncommon phenomenon, as it has been observed in other basaltic volcanoes [e.g., Lamb et al., 2022].

Also the ratio between seismic and infrasonic amplitude was computed at both ECPN and EMFO (Fig. 11). This analysis was performed only during the lava fountain episodes, as the infrasonic signal can strongly be affected by noise during non-eruptive periods. The most important result from this analysis is the low level of seismic/infrasonic amplitude ratio obtained in the last episode compared to the others. As suggested by Johnson and Aster [2005], many different factors can affect and modify the seismo-acoustic energy partitioning on active volcanoes such as changes in magma properties, conduit obstruction, fragmentation depths, topographic effects (especially influencing the infrasonic amplitude as recorded by the infrasonic stations) and so on. In this case, it is evident how the observed low value of the seismic/infrasonic amplitude ratio is due to the sharp increase in the infrasonic radiation during the fourth episode (much sharper than the seismic increase; see Fig.s 2a and 7a). This could likely result from variations in the conditions of the upper part of the plumbing system.

3.3 Tremor source location

The results obtained using the amplitude-based grid-search method for volcanic tremor localization reveal seismic sources located in the northwest-southeast direction along the summit area of Mount Etna (Fig. 12a). Similar to what shown in previous recent works [e.g. Calvari et al., 2022; Sciotto et al., 2022a], most of the located sources are found at a depth equal to or less than 1 km with respect to the volcano's summit, including the tremors recorded during the paroxysmal episodes, which are located about 3 kilometers above sea level (that is, very close to the topographical surface). The fact that volcanic tremor sources are located in such a shallow zone indicates that the magmatic and degassing activity, releasing most of energy, within the plumbing system takes place near the summit craters.

During the period prior to the four studied paroxysmal events, which spanned from February 14 to 16, characterized by a large seismic tremor amplitude (Fig. 2a, b), the source of the seismic tremors was located at shallow depth beneath the SEC (Figs. 12, 13a-b). According to the model proposed by Girona et al. [2019], the shallow structure of the magma plumbing system is likely to be divided into three regions: a deeper zone housing the liquid magma reservoir where gas bubbles ascend, an intermediate zone with a gas pocket, and a superficial zone with a permeable solid layer. This model allows us to approximate the situation of the plumbing system beneath the SEC shortly before the eruption and explain the origin of the seismic tremor as due to the flow of

gasses through the permeable solid layer and the accumulation of gasses beneath that layer [Girona et al., 2019]. During the non-eruptive periods between the four paroxysmal episodes, the amplitude of volcanic tremors decreases significantly, and their source shifts towards the central craters, meaning that volcanic tremor source below this area is predominant or more energetic in this time interval (Figs. 12 and 13a, b). Regarding the origin of the seismic sources, the same model mentioned earlier can be applied to this non-eruptive volcanic tremor, located in the shallow conduits of the central craters. The source of the volcanic tremor during lava fountains is located beneath the crater where the eruptions occurred, the SEC (Figs. 12 and 13). Furthermore, as mentioned earlier, this tremor exhibits a greater amplitude compared to the remaining period. In this case, the features of volcanic tremor together with the open conduit conditions lead us to infer a different model to explain the eruptive volcanic tremor source: it can be attributed to the vibration caused by the turbulent upward flow of magma and the impact of particles on the conduit walls [Gestrich et al., 2020].

In addition, it is worth noting that, when the volcanic tremor localization moves forward and backward at so shallow depth, the source migration is only apparent, and it is likely that there are, at least, two sources of volcanic tremor, related to craters differently active over time. In our case study, these are the central craters (VOR and BN) and the SEC. Consequently, location apparently moves towards the most active crater area at that time.

It is important to highlight that there is a slight but progressive migration of volcanic tremor sources towards the eastern portion of the summit area as the four lava fountains occur, as depicted in Figures 13a and 14. This observation aligns perfectly with the observations reported in the Bulletins published by the INGV regarding these eruptions (https://www.ct.ingv.it/index.php/monitoraggio-e-sorveglianza/prodotti-del-monitoraggio/bollettini-settimanali-multidisciplinari), which indicate the formation of eruptions vents in the eastern part of the SEC as the paroxysmal episodes progress.

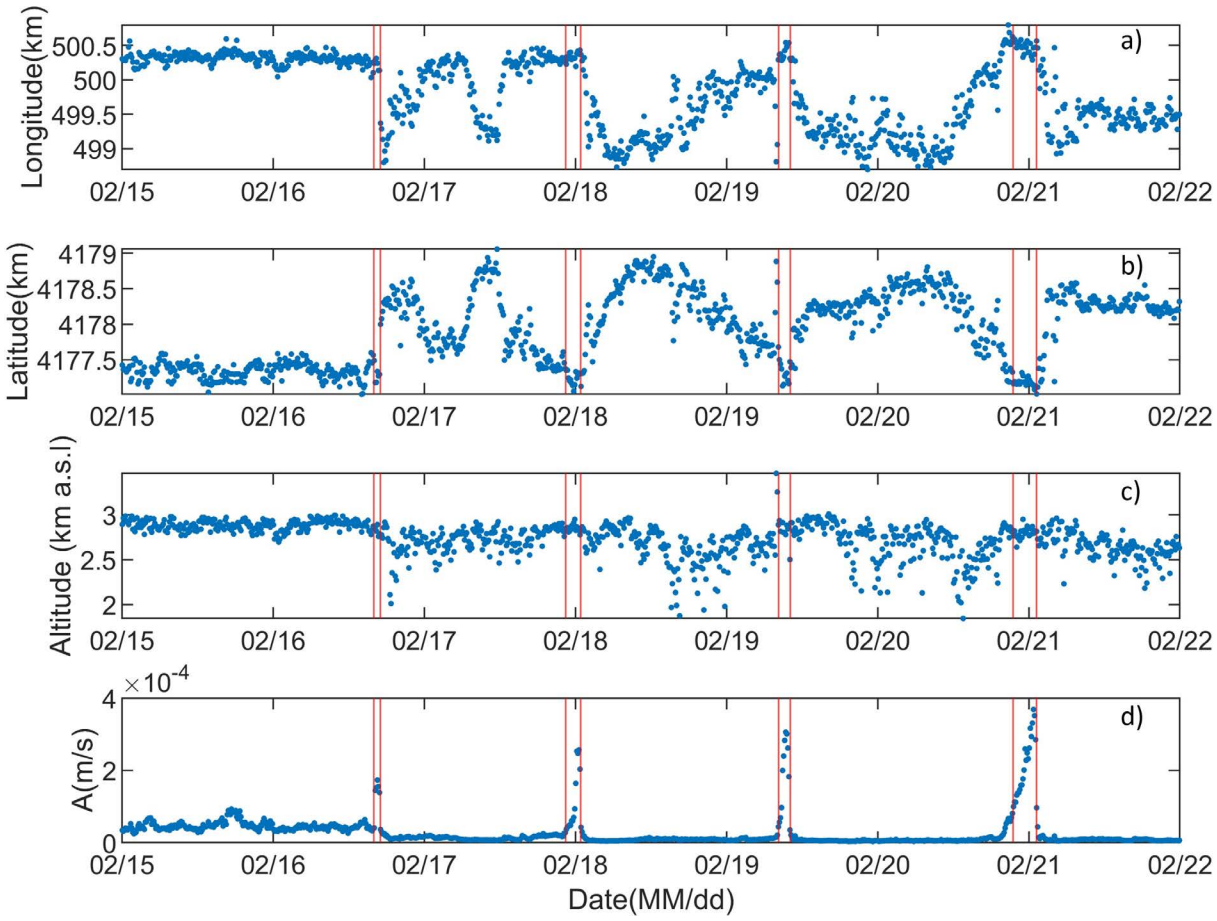

Figure 13. Time variation of longitude (a), latitude (b), altitude (c) and reduced amplitude (d) computed for the volcanic tremor source location. The times of occurrence of the lava fountain episodes are marked by red vertical lines. As depicted in Figure 12, the tremor source location and reduced amplitude have not been computed on February 14th.

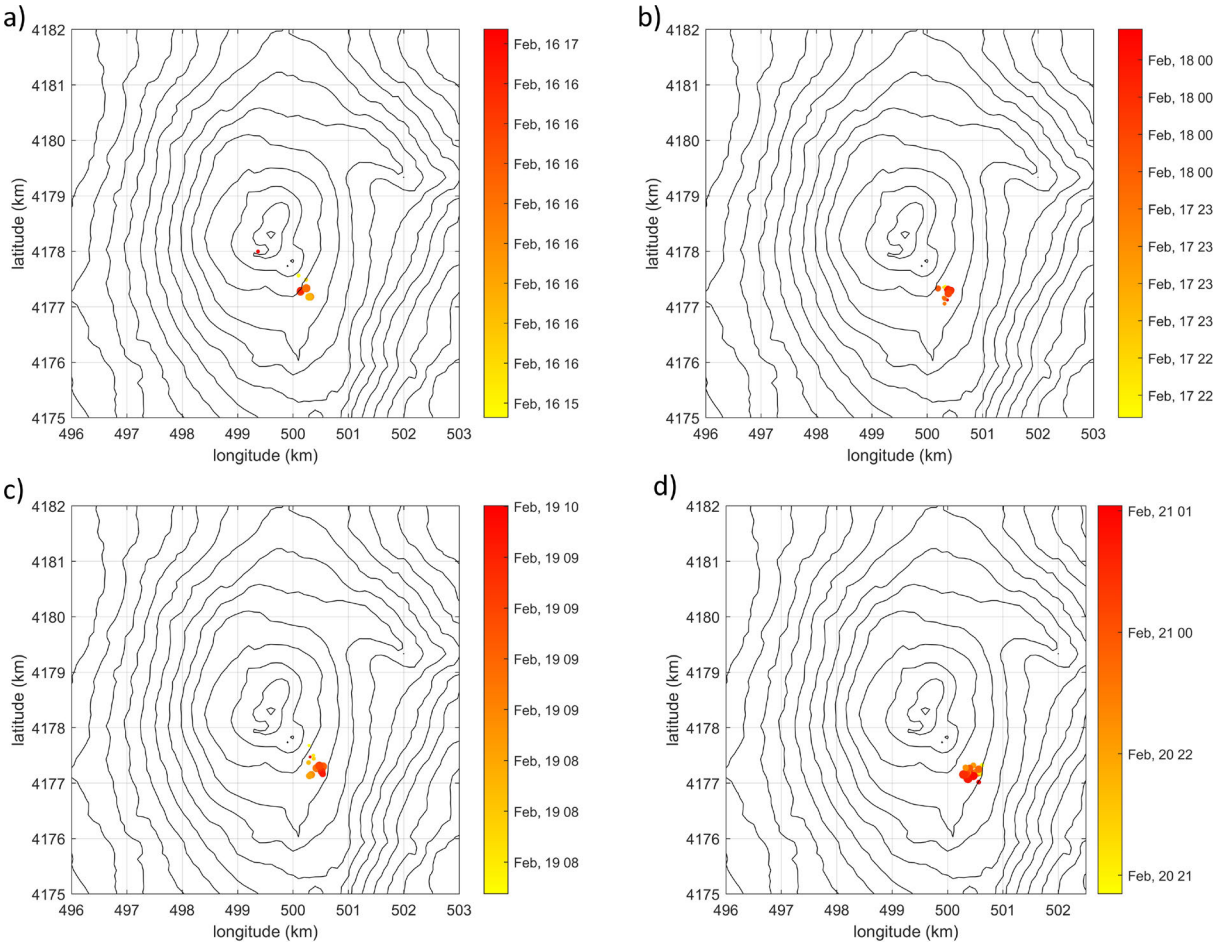

Figure 14. Maps of Mt. Etna showing the location of volcanic tremor sources during the four episodes of lava fountain (dots). The size of the dots depend on the seismic reduced amplitude, the colors on the time (see the colorbar).

4. Concluding remarks

In this work, seismic and infrasonic signals recorded between February 14th and 21st, 2021, during intense explosive activity, primarily involving four lava fountain episodes from SEC, have been analyzed. These are the main findings of this work:

- As previously shown by other works [e.g. Andronico et al., 2021; Calvari et al., 2022], the pattern followed by the RMS amplitude, in both seismic and infrasonic signals, helps track the evolution in time of the volcano activity, being characterized by a marked increase during the lava fountain episodes, followed by significantly lower values during the periods between them.
- By comparing the maximum values of seismic amplitude reached during each lava fountain event with the volume of magma emitted in these events, a direct relationship is observed. However, this relationship does not apply to the infrasonic amplitude, as the latter depends on many factors not only related to the volcano dynamics but also to topography and atmospheric parameters.
- The seismic volcanic tremor sources turn out to be located below the most active summit crater (SEC) at shallow depth for most of the analyzed period. It is also worth noting that the volcanic tremor sources progressively migrate further east during the four lava fountains, in agreement with the volcanological observations indicating the formation of eruptive vents in the eastern part of the SEC as the paroxysmal episodes progress.
- During the studied week, the energy released by seismic tremor is predominantly below 5.0 Hz. During lava fountain episodes, the ECPN station shows frequencies that do not exceed 4.0 Hz, while the EMFO station records frequencies which do not exceed 3.0 Hz. Both frequency ranges drop during paroxysmal phases. This spectral difference is due to the more distant location of the EMFO station with respect to the seismic tremor sources and then to propagation effects.

Acknowledgements. We are indebted to the technicians of the INGV, Osservatorio Etneo, for enabling acquisition of the infrasound and seismic data. A.C. thanks the grant PIACERI, 2020-22 programme, Università degli Studi di Catania (PAROSSISMA project, code 22722132140; principal investigator Marco Viccaro). M.S., G.D.G. and A.C. thank the IMPACT project—a multidisciplinary Insight on the kinematics and dynamics of Magmatic Processes at Mt. Etna Aimed at identifying preCursor phenomena and developing early warning sysTems, funded by INGV-Progetto Strategico Dipartimento Vulcani 2019 (Delibera n. 144/2020).

References

Almendros, J., J.M. Ibañez, G. Alguacil, E. Del Pezzo and R. Ortiz (1997). Array tracking of the volcanic tremor source at Deception Island, Antarctica, Geophys. Res. Lett. 24, 3069-3072. Doi: 10.1029/97GL03096

Alparone, S., D. Andronico, L. Lodato and T. Sgroi (2003). Relationship between tremor and volcanic activity during the Southeast Crater eruption on Mount Etna in early 2000, J. Geophys. Res., 108, 2241, doi:10.1029/2002JB001866

Alparone, S., A. Cannata and S. Gresta (2007). Time variation of spectral and wavefield features of volcanic tremor at Mt. Etna (January-June 1999), J. Vol. Geoth. Res., 161, 4, 318-332 doi:10.1016/j.jvolgeores.2006.12.012

Andronico, D., A. Cannata, G. Di Grazia, and F. Ferrari (2021). The 1986-2021 paroxysmal episodes at the summit craters of Mt. Etna: Insights into volcano dynamics and hazard, Earth-Sci. Rev., 220, 103686. doi: 10.1016/j.earscirev.2021.103686

Battaglia, J. and K. Aki (2003). Location of seismic events and eruptive fissures on the Piton de la Fournaise volcano using seismic amplitudes, J. Geophys. Res., 108, B8, 2364, DOI: 10.1029/2002JB002193

Battaglia, J., K. Aki and V. Ferrazzini (2005). Location of tremor sources and estimation of lava output using tremor source amplitude on the Piton de la Fournaise volcano: 1. Location of tremor sources, J. Vol. Geoth. Res., 147, 3-4, 268-290, doi:10.1016/j.jvolgeores.2005.04.005

Benoit, J.P. and S.R. McNutt (1997). New constraints on source processes of volcanic tremor at Arenal Volcano, Costa Rica, using broadband seismic data, Geophys. Res. Lett., 24, 449-452, doi: 10.1029/97GL00179

Buzzard, Q., J.B. Langman, D. Behrens and J.G. Moberly (2023). Monitoring the Ambient Seismic Field to Track Groundwater at a Mountain-Front Recharge Zone, Geosciences, 13, 1, 9, doi: 10.3390/geosciences13010009

Calvari, S. and G. Nunnari (2022). Comparison between automated and manual detection of lava fountains from fixed monitoring thermal cameras at Etna Volcano, Italy, Remote Sensing, 14, 10, 2392, doi: 10.3390/rs14102392

Calvari, S, E. Biale, A. Bonaccorso, A. Cannata, L. Carleo, G. Currenti, G. Di Grazia, G. Ganci, A. Iozzia, E. Pecora, et al. (2022). Explosive Paroxysmal Events at Etna Volcano of Different Magnitude and Intensity Explored through a Multidisciplinary Monitoring System, Remote Sensing, 14, 16, 4006, doi: 10.3390/rs14164006

Cannata, A., A. Catania, S. Alparone and S. Gresta (2008). Volcanic tremor at Mt. Etna: Inferences on magma dynamics during effusive and explosive activity, J. Vol. Geoth. Res., 178, 1, 19-31, doi: 10.1016/j.jvolgeores.2007.11.027

Cannata, A., G. Di Grazia, P. Montalto, F. Ferrari, G. Nunnari, D. Patanè and E. Privitera (2010). New insights into banded tremor from the 2008-2009 Mount Etna eruption, J. Geophys. Res.: Solid Earth, 115, B12, doi: 10.1029/2009JB007120

Cannata, A., G. Di Grazia, M. Aliotta, C. Cassisi, P. Montalto and D. Patanè (2013). Monitoring seismo-volcanic and infrasonic signals at volcanoes: Mt. Etna case study, Pure Appl. Geophys., 170, 1751-1771, DOI: 10.1007/s00024-012-0634-x

Cannavò, F., A. Cannata, C. Cassisi, G. Di Grazia, P. Montalto, M. Prestifilippo, … and S. Gambino (2017). A multivariate probabilistic graphical model for real-time volcano monitoring on Mount Etna, J. Geophys. Res.: Solid Earth, 122, 5, 3480-3496, doi: 10.1002/2016JB013512

Carniel, R., E. Del Pin, R. Budai and P. Pascolo (2005). Identifying timescales and possible precursors of the awake to asleep transition in EOG time series, Chaos Solit. Fract., 23, 1259-504 1266, doi: 10.1016/j.chaos.2004.06.021

Cassisi, C., M. Prestifilippo, A. Cannata, P. Montalto, D. Patanè and E. Privitera (2016). Probabilistic reasoning over seismic time series: Volcano monitoring by hidden Markov models at Mt. Etna, Pure Appl. Geophys., 173, 2365-2386, DOI: 10.1007/s00024-016-1284-1

Chouet, B. (1996). Long-period volcano seismicity: its source and use in eruption forecasting, Nature, 380, 309-316. doi: 10.1038/380309a0

Chouet, B.A. and R.S. Matoza (2013). A multi-decadal view of seismic methods for detecting precursors of magma movement and eruption, J. Vol. Geoth. Res., 252, 108-175, doi: 10.1016/j.jvolgeores.2012.11.013

D'Alessandro, W. and F. Vita (2003). Groundwater radon measurements in the Mt. Etna area, J. Enviro. Radioact., 65, 2, 187-201, doi: 10.1016/s0265-931x(02)00096-6

D'Agostino, M., G. Di Grazia, F. Ferrari, H. Langer, A. Messina, D. Reitano and S. Spampinato (2013). Volcano Monitoring and Early Warning on Mt Etna Based on Volcanic Tremor—Methods and Technical Aspects, Nova Science Publishers, New York, NY, USA, 4, 53-92. https://www.novapublishers.com/catalog/product_info.php?products_id=42535

Di Grazia, G., S. Falsaperla and H. Langer (2006), Volcanic tremor location during the 2004 Mount Etna lava effusion, Geophysical Research Letters, 33, L04304, doi: 10.1029/2005GL025177

Endo, E.T. and T. Murray (1991). Real-time seismic amplitude measurement (RSAM): a volcano monitoring and prediction tool, Bull. Vol., 53, 533-545, doi: 10.1007/BF00298154

Falsaperla, S., S. Alparone, S. D'Amico, G. Di Grazia, F. Ferrari, H. Langer … and S. Spampinato (2005). Volcanic tremor at Mt. Etna, Italy, preceding and accompanying the eruption of July-August, 2001, Pure Appl. Geophys., 162, 2111-2132, doi: 10.1007/s00024-005-2710-y

Fee, D., M. Garcés, M. Patrick, B. Chouet, P. Dawson, and D. Swanson (2010), Infrasonic harmonic tremor and degassing bursts from Halema'uma'u Crater, Kilauea Volcano, Hawaii, J. Geophys. Res., 115, B11316, doi: 10.1029/2010JB007642

Fee, D. and R.S. Matoza (2013). An overview of volcano infrasound: From Hawaiian to Plinian, local to global, J. Vol. Geoth. Res., 249, 123-139, doi: 10.1016/j.jvolgeores.2012.09.002

Gestrich, J.E., D. Fee, V.C. Tsai, M.M. Haney, and A.R. Van Eaton (2020). A physical model for volcanic eruption tremor, J. Geophys. Res.: Solid Earth, 125, e2019JB018980, doi: 10.1029/2019JB018980

Girona, T., C. Caudron and C. Huber (2019). Origin of shallow volcanic tremor: The dynamics of gas pockets trapped beneath thin permeable media, J. Geophys. Res.: Solid Earth, 124, 4831-4861, doi: 10.1029/2019JB017482

Gordeev, E. (1993). Modeling of volcanic tremor as explosive point sources in a single-layered, elastic half-space, J. Geophys. Res.: Solid Earth, 98, B11, 19687-19703, doi: 10.1029/93JB00348

Guerrieri, L., S. Corradini, N. Theys, D. Stelitano and L. Merucci (2023). Volcanic clouds characterization of the 2020-2022 sequence of Mt. Etna lava fountains using MSG-SEVIRI and products' cross-comparison, Remote Sensing, 15, 8, 2055, DOI: 10.3390/rs15082055

Ibáñez, J., and E. Carmona (2000). Sismicidad Volcánica, Instituto Andaluz de Geofísica, Universidad de Granada. 242584653_SISMICIDAD_VOLCANICA

Ichihara, M. (2016), Seismic and infrasonic eruption tremors and their relation to magma discharge rate: A case study for sub-Plinian events in the 2011 eruption of Shinmoe-dake, Japan, J. Geophys. Res.: Solid Earth, 121, 10, 7101-7118, doi: 10.1002/2016JB013246

Iozzia, A., L.M. Watson, M. Cantarero, E. De Beni, G. Di Grazia, G. Ganci, … and A. Cannata (2023). The influence of volcano topographic changes on infrasound amplitude: lava fountains at Mt. Etna in 2021, Bull. Vol., 85, 10, 1-19, doi: 10.1007/s00445-023-01672-x

Johnson, J.B., R.C. Aster and P.R. Kyle (2004). Volcanic eruptions observed with infrasound, Geophys. Res. Lett., 31, L14604, doi: 10.1029/2004GL020020

Johnson, J.B., and R.C. Aster (2005). Relative partitioning of acoustic and seismic energy during Strombolian eruptions, Journal of Vol. Geoth. Res., 148, 3-4, 334-354, DOI: 10.1016/j.jvolgeores.2005.05.002

Johnson, J.B. and M. Ripepe (2011). Volcano infrasound: A review, J. Vol. Geoth. Res., 206, 3-4, 61-69, doi: 10.1016/j.jvolgeores.2011.06.006

Kao, H. and S.-J. Shan (2004). The Source-Scanning Algorithm: mapping the distribution of seismic sources in time and space, Geophys. J. Int., 157, 2, 589-594, doi: 10.1111/j.1365-246X.2004.02276.x

Konstantinou, K.I. and V. Schlindwein (2003). Nature, wavefield properties and source mechanism of volcanic tremor: a rew, J. Vol. Geoth. Res., 119, 1-4, 161-187, doi: 10.1016/S0377-0273(02)00311-6

Lamb, O.D., J.E. Gestrich, T.D. Barnie, et al. (2022). Acoustic observations of lava fountain activity during the 2021 Fagradalsfjall eruption, Iceland, Bull. Vol., 84, 96, doi: 10.1007/s00445-022-01602-3

Langer, H., S. Falsaperla, S. Spampinato, et al. (2022). Energy threshold changes in volcanic activity at Mt. Etna (Italy) inferred from volcanic tremor, Sci. Rep., 12, 17895, doi: 10.1038/s41598-022-20766-8

Lombardo, G., G. Coco, M. Corrao and S. Gresta (1996). Features of seismic events and volcanic tremor during the preliminary stages of the 1991-1993 eruption of Mt. Etna, https://api.semanticscholar.org/CorpusID:126542512

Marchese, F., C. Filizzola, T. Lacava, A. Falconieri, M. Faruolo, N. Genzano, … and M. Neri (2021). Mt. Etna paroxysms of February-April 2021 monitored and quantified through a multi-platform satellite observing system, Remote Sensing, 13(16), 3074. DOI: 10.3390/rs13163074

Matoza, R.S., D. Fee, M.A. Garcés, J.M. Seiner, P.A. Ramón and M.A.H. Hedlin (2009). Infrasonic jet noise from volcanic eruptions, Geophys. Res. Lett., 36, L08303, doi: 10.1029/2008GL036486

Matoza, R.S. and D.C. Roman (2022). One hundred years of advances in volcano seismology and acoustics, Bull. Vol., 84, 86, doi: 10.1007/s00445-022-01586-0

McNutt, S.R. and T. Nishimura (2008). Volcanic tremor during eruptions: temporal characteristics, scaling and constraints on conduit size and processes, J. Vol. Geoth. Res., 178, 1, 10-18, doi: 10.1016/j.jvolgeores.2008.03.010

Mora, M.M., P. Lesage, J. Dorel, P.Y. Bard, J.P. Métaxian, G.E. Alvarado and C. Leandro (2001). Study of seismic site effects using H/V spectral ratios at Arenal Volcano, Costa Rica, Geophys. Res. Lett., 28, 15, 2991-2994, doi: 10.1029/2001GL013049

Neri, M., M. De Maio, S. Crepaldi, E. Suozzi, M. Lavy, F. Marchionatti, S. Calvari and M.F. Buongiorno (2017). Topographic maps of Mount Etna's summit craters, updated to December 2015, J. Maps, 13, 2, 674-683, doi: 10.1080/17445647.2017.1352041

Patanè, D., O. Cocina, S. Falsaperla, E. Privitera and S. Spampinato (2004). Mt. Etna volcano: A seismological framework, in Mt. Etna: Volcano Laboratory, edited by A. Bonaccorso, S. Calvari, M. Coltelli, C. Del Negro and S. Falsaperla, doi: 10.1029/143GM10

Patanè, D., et al. (2013). Insights into magma and fluid transfer at Mount Etna by a multiparametric approach: A model of the events leading to the 2011 eruptive cycle, J. Geophys. Res.: Solid Earth, 118, 3519-3539, doi: 10.1002/jgrb.50248

Pioli, L., M. Palmas, B. Behncke, E. De Beni, M. Cantarero and S. Scollo (2022). Quantifying strombolian activity at Etna Volcano, Geosciences, 12, 4, 163, doi: 10.3390/geosciences12040163

Pulli, J. J. (1984). Attenuation of coda waves in New England, Bull. Seismol. Soc. Am., 74, 4, 1149-1166, doi: 10.1785/BSSA0740041149

Sciotto, M., A. Cannata, S. Gresta, E. Privitera and L. Spina (2013). Seismic and infrasound signals at Mt. Etna: Modeling the North-East crater conduit and its relation with the 2008-2009 eruption feeding system, J. Vol. Geoth. Res., 254, 53-68, doi: 10.1016/j.jvolgeores.2012.12.024

Sciotto, M., A. Cannata, M. Prestifilippo, et al. (2019). Unravelling the links between seismo-acoustic signals and eruptive parameters: Etna lava fountain case study, Sci. Rep., 9, 16417, doi: 10.1038/s41598-019-52576-w

Sciotto, M., A. Cannata, G. Di Grazia and P. Montalto (2022a). Volcanic tremor and long period events at Mt. Etna: Same mechanism at different rates or not?, Phys. Earth Planet. Int., 324, 106850, doi: 10.1016/j.pepi.2022.106850

Sciotto, M., L.M. Watson, A. Cannata, M. Cantarero, E. De Beni and J.B. Johnson (2022b). Infrasonic gliding reflects a rising magma column at Mount Etna (Italy), Sci. Rep., 12, 1, 16954, doi: 10.1038/s41598-022-20258-9

Spampinato, L., M. Sciotto, A. Cannata, F. Cannavò, A. La Spina, M. Palano … and T. Caltabiano (2015). Multiparametric study of the February-April 2013 paroxysmal phase of Mt. Etna New South-East crater, Geochem., Geophys., Geosys., 16, 6, 1932-1949, doi: 10.1002/2015GC005795

Steinberg, G.S. and A.S. Steinberg (1975), On possible causes of volcanic tremor, J. Geophys. Res., 80, 11, 1600-1604, doi: 10.1029/JB080i011p01600

Tribaldos, V.R. and J.B. Ajo-Franklin (2021). Aquifer monitoring using ambient seismic noise recorded with distributed acoustic sensing (DAS) deployed on dark fiber, J. Geophys. Res.: Solid Earth, 126, e2020JB021004, doi: 10.1029/2020JB021004

***CORRESPONDING AUTHOR: Javier MARTÍNEZ MORENO**,
Department of Theoretical Physics and Cosmos, University of Granada, Avenida de la Fuente Nueva S/N, 18071, Granada, Spain
e-mail: javimarmo@correo.ugr.es